# Characterization and Computation of the Feasible Space of an Articulated Probe

**Ovidiu Daescu and Ka Yaw Teo**

**Department of Computer Science, University of Texas at Dallas, Richardson, TX, USA**
{ovidiu.daescu, ka.teo}@utdallas.edu

**Abstract**

We present an efficient algorithm for computing the feasible solution space for a trajectory planning problem involving an articulated two-link probe constrained to a fixed sequence of motions – a straight line insertion, possibly followed by a rotation of the end link. Given $n$ line segment obstacles in the workspace, we show that the feasible trajectory space of the articulated probe can be characterized by an arrangement of simple curves of complexity $O(k)$, which can be constructed in $O(n \log n + k)$ time using $O(n+k)$ space, where $k = O(n^2)$ is the number of vertices of the arrangement. Additionally, our solution approach produces a new data structure for solving a special case of the circular sector intersection query problem.

## 1 Introduction

In minimally invasive surgeries, a rigid needle-like robotic arm is typically inserted through a small incision to reach its given target, after which it may perform operations such as tissue resection and biopsy. Some newly developed variants allow for a joint to be close to the acting end (tip) of the arm; after inserting the arm in a straight path, the surgeon may rotate the tip around the joint to reach the target. This enhances the ability to reach deep targets but greatly increases the complexity of finding acceptable insertion/rotation pairs.

Unlike polygonal linkages that can rotate freely at the joints while moving between a start and target configuration [2, 8, 9], a simple articulated probe is constrained to a fixed sequence of moves – a straight line insertion, possibly followed by a rotation of the short link. This type of motion has not received attention until very recently [3, 4].

As originally proposed in [4], an articulated probe is modeled in $\Re^2$ as two line segments, $ab$ and $bc$, joined at point $b$. The length of $ab$ can be arbitrarily large (infinitely long), while $bc$, corresponding to the tip of the probe, has a fixed length $r$. A two-dimensional workspace (see Figure 1) is given by the region bounded by a large circle $S$ of radius $R$ centered at $t$, enclosing a set $P$ of $n$ disjoint line segment obstacles and a target point $t$ in the free space.

At the start, the probe is outside $S$ and assumes an *unarticulated* configuration, in which $ab$ and $bc$ are collinear, with $b \in ac$. A *feasible probe trajectory* consists of an initial insertion of straight line segment $abc$, possibly followed by a rotation of $bc$ at $b$ up to $\pi/2$ radians in either direction, such that point $c$ ends at $t$, while avoiding obstacles in the process. If a rotation is performed, then we have an *articulated final* configuration of the probe.

The objective of this paper is to characterize and compute the feasible trajectory space (i.e., set of all feasible trajectories) of the articulated probe.

**Previous work.** The articulated probe problem in two dimensions was formally introduced in [4], where an algorithm was presented for finding so-called *extremal* feasible probe trajectories in $O(n^2 \log n)$ time using $O(n \log n)$ space. In an extremal probe trajectory, the probe is tangent to one or two obstacle endpoints. Later, it was shown in [3] that, for any constant $\delta > 0$, a feasible probe trajectory with a clearance $\delta$ from the obstacles can be determined in $O(n^2 \log n)$ time using $O(n^2)$ space.

35th European Workshop on Computational Geometry, Utrecht, The Netherlands, March 18–20, 2019.
This is an extended abstract of a presentation given at EuroCG'19. It has been made public for the benefit of the community and should be considered a preprint rather than a formally reviewed paper. Thus, this work is expected to appear eventually in more final form at a conference with formal proceedings and/or in a journal.

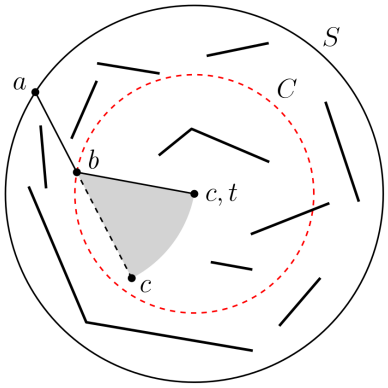


**Figure 1** Trajectory planning for an articulated probe. In order to reach point $t$, a straight insertion of line segment $abc$ may be followed by a rotation of line segment $bc$ from its intermediate position (black dashed line) to the final position (black solid line).

**Results and contributions.** We describe a geometric combinatorial approach for characterizing and computing the feasible trajectory space of the articulated probe. The feasible configuration space has worst-case complexity of $O(n^2)$ and can be described by an arrangement of simple curves. By using the topological sweep method [1], the arrangement can be constructed in $O(n \log n + k)$ time using $O(n + k)$ working storage, where $k$ is the number of vertices of the arrangement. Our approach also results in a simplified data structure of similar space/time complexity compared to that in [4] for solving a special instance of the *circular sector intersection query* problem (i.e., for a query circular sector with a fixed radius $r$ and a fixed arc endpoint $t$).

## 2 Solution approach

We characterize 1) the final configuration space, 2) the *forbidden* final configuration space, and 3) the *infeasible* final configuration space, as detailed in this section.

### 2.1 Final configuration space

In a final configuration of the articulated probe, point $a$ can be assumed to be located on $S$, and point $b$ lies on a circle $C$ of radius $r$ centered at $t$ (see Figure 1). Let $\theta_S$ and $\theta_C$ be the angles of $ta$ and $tb$ relative to the $x$-axis, respectively, where $\theta_S, \theta_C \in [0, 2\pi)$. Since $bc$ may rotate as far as $\pi/2$ radians in either direction, for any given $\theta_S$, we have $\theta_C \in [\theta_S - \cos^{-1} r/R, \theta_S + \cos^{-1} r/R]$. We call this the *unforbidden* range of $\theta_C$. A final configuration of the articulated probe can be specified by a two-tuple $(\theta_S, \theta_C)$, depending on the locations of points $a$ and $b$ on circles $S$ and $C$, respectively (see Figure 2). The final configuration space $\Sigma_{fin}$ of the articulated probe can be computed in $O(1)$ time.

### 2.2 Forbidden final configuration space

A final configuration is called *forbidden* if the final configuration (represented by $ab$ and $bt$) intersects with one or more of the obstacle line segments. The following two cases arise.

**Case 1. Obstacle line segment $s$ outside $C$.** The corresponding forbidden final configuration space can be characterized as follows. Let angles $\theta_i$, where $i = 1, \ldots, 6$, be defined

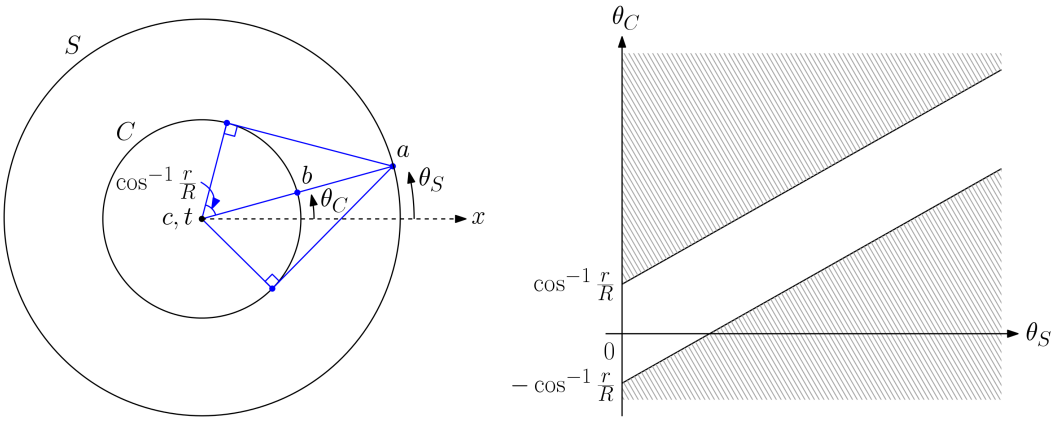


**Figure 2** Final configurations of the probe. The unshaded region of the $(\theta_S, \theta_C)$-plot represents the unforbidden final configuration space when the workspace contains no obstacles.

in the manner depicted in Figure 3. Briefly, each $\theta_i$ corresponds to an angle $\theta_S$ at which point a tangent line between $C$ and $s$, or from $t$ to $s$, intersects $S$. As $\theta_S$ increases from $\theta_1$ to $\theta_3$, the upper bound of the unforbidden range of $\theta_C$ decreases as a continuous function of $\theta_S$. Similarly, when $\theta_S$ varies from $\theta_4$ to $\theta_6$, the lower bound of the unforbidden range of $\theta_C$ decreases as a continuous function of $\theta_S$. For $\theta_3 \leq \theta_S \leq \theta_4$, there exists no unforbidden final configuration at any $\theta_C$. For conciseness, the upper (resp. lower) bound of the unforbidden range of $\theta_C$ is simply referred to as the upper (resp. lower) bound of $\theta_C$ hereafter.

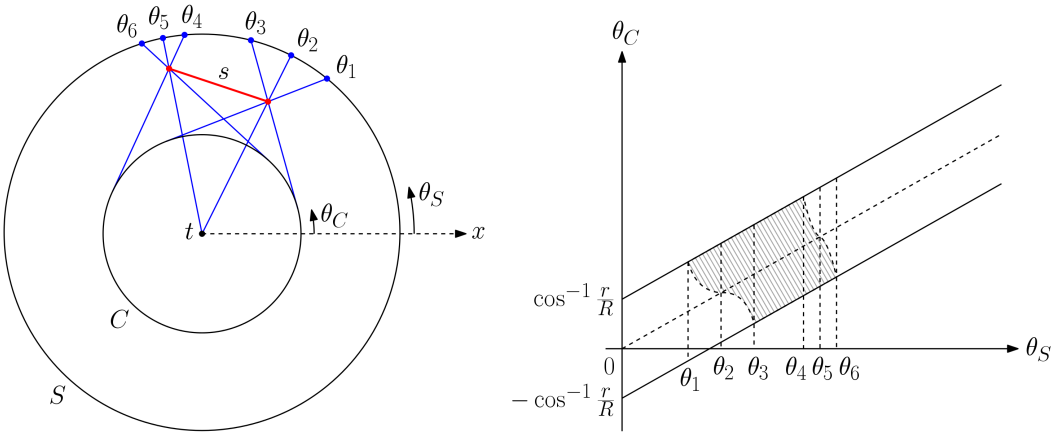


**Figure 3** Forbidden final configurations due to an obstacle line segment $s$ outside $C$.

**Case 2. Obstacle line segment $s$ inside $C$.** We compute the forbidden final configuration space for $s$ in a similar way. Note that, as shown in Figure 4, angles $\theta_i$ (where $i = 1, \ldots, 6$) are defined differently from the previous case. For $\theta_1 \leq \theta_S \leq \theta_4$, the upper bound of $\theta_C$ is equivalent to $\theta_2$. For $\theta_3 \leq \theta_S \leq \theta_6$, the lower bound of $\theta_C$ equals to $\theta_5$.

We can find the forbidden final configuration space for an obstacle line segment (i.e., final configuration obstacle) in $O(1)$ time. Thus, for $n$ obstacle line segments, it takes a total of $O(n)$ time to compute the corresponding set of configurations. The union of these configurations forms the forbidden final configuration space $\Sigma_{fin,forb}$ of the articulated probe.

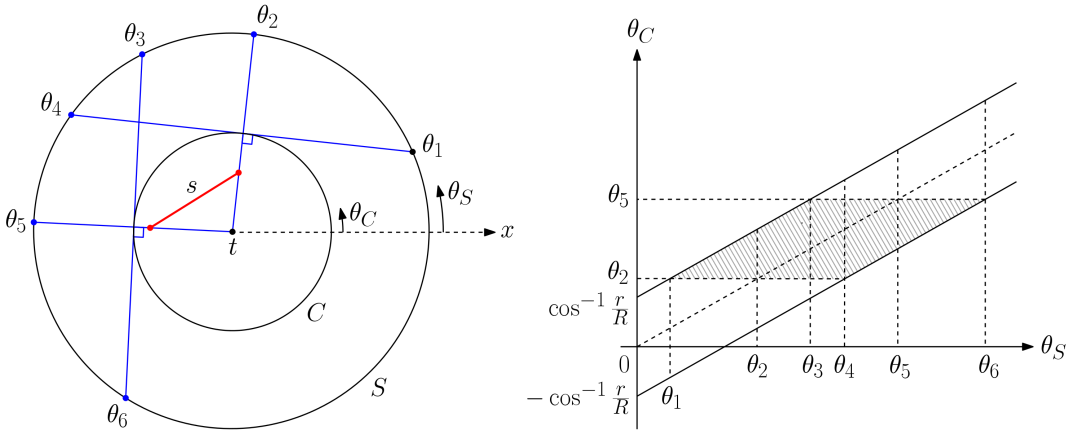


**Figure 4** Forbidden final configurations due to an obstacle line segment $s$ inside $C$.

The free final configuration space $\Sigma_{fin,free}$ of the articulated probe is the complement of $\Sigma_{fin,forb}$; that is, $\Sigma_{fin,free} = \Sigma_{fin} \setminus \Sigma_{fin,forb}$.

## 2.3 Infeasible final configuration space

The feasible trajectory space of the articulated probe can be characterized as a subset of $\Sigma_{fin,free}$. A final configuration is called *infeasible* if the circular sector associated with the final configuration (i.e., the area swept by segment $bc$ to reach target point $t$) intersects with any obstacle line segment. We denote the infeasible final configuration space as $\Sigma_{fin,inf}$.

Let $C'$ be a circle centered at $t$ and of radius $\sqrt{2}r$. A circular sector associated with a final configuration can only intersect with an obstacle line segment lying inside $C'$. In contrast to characterizing the lower and upper bounds of $\theta_C$ as $\theta_S$ varies from 0 to $2\pi$ as in the prior section, we herein perform the characterization in reverse. For conciseness, we only present arguments for the negative half of the $\theta_S$-range, which is $[\theta_C - \cos^{-1} r/R, \theta_C]$, and the similar arguments apply to the other half due to symmetry. As before, two cases arise.

**Case 1. Obstacle line segment $s$ inside $C$.** As shown in Figure 5, we are only concerned with computing the lower bound of $\theta_S$ for $\theta_C \in [\phi_1, \phi_2]$, given that the entire negative half of the $\theta_S$-range (i.e., $[\theta_C - \cos^{-1} r/R, \theta_C]$) is feasible for $\theta_C \in [0, \phi_1] \cup [\phi_3, 2\pi)$, and is infeasible for $\theta_C \in [\phi_2, \phi_3]$ due to intersection of $bt$ with $s$.

For brevity, the quarter-circular sector associated with a point $b$ (i.e., the maximum possible area swept by segment $bc$ to reach point $t$), where the angle of $tb$ (relative to the $x$-axis) is $\theta_C$, is henceforth referred to as the *quarter-circular sector associated with* $\theta_C$.

$\phi_1$, $\phi_2$ and $\phi_3$ can be described in brief as follows (see Figure 5a). $\phi_1$ is the smallest angle $\theta_C$ at which the circular arc (of the quarter-circular sector associated with $\theta_C$) intersects with $s$ (at one of its endpoints or interior points). $\phi_2$ is the smallest angle $\theta_C$ at which $bt$ (of the quarter-circular sector associated with $\theta_C$) intersects with $s$ (at one of its endpoints). $\phi_3$ is the largest angle $\theta_C$ at which $bt$ (of the quarter-circular sector associated with $\theta_C$) intersects with $s$ (at one of its endpoints). In other words, as $\theta_C$ varies from 0 to $2\pi$, $\phi_1$ and $\phi_3$ are the angles $\theta_C$ at which the quarter-circular sector associated with $\theta_C$ first and last intersects with $s$, respectively.

For $\theta_C \in [\phi_1, \phi_2]$, the lower bound of $\theta_S$ can be represented by a piecewise continuous curve, which consists of at most two pieces, corresponding to two intervals $[\phi_1, \alpha]$ and $[\alpha, \phi_2]$,

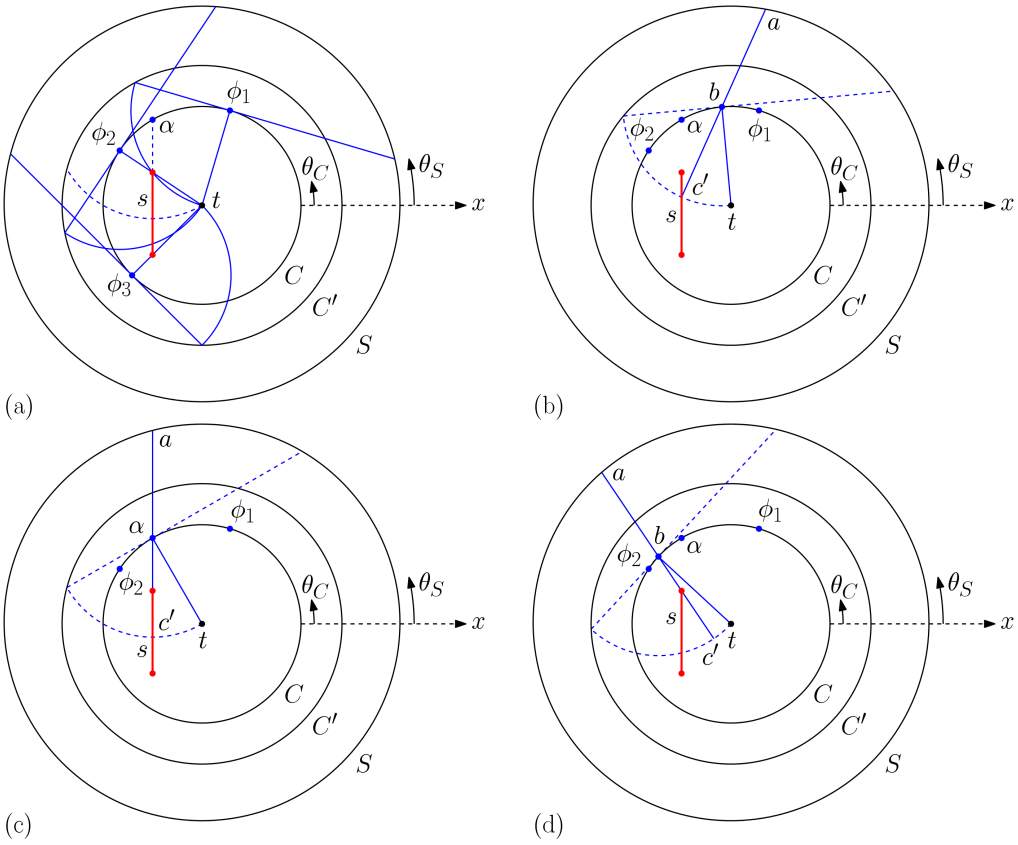


**Figure 5** Infeasible final configurations due to an obstacle line segment $s$ inside $C$. Illustration of $\theta_S$-lower bound for (a) $\theta_C \in [\phi_1, \phi_2]$, (b) $\phi_1 < \theta_C < \alpha$, (c) $\theta_C = \alpha$, and (d) $\alpha < \theta_C < \phi_2$.

where $\alpha$ is the angle $\theta_C$ of the intersection point between $C$ and the supporting line of $s$. Note that, if $\phi_1 \leq \alpha$, then the lower-bound curve of $\theta_S$ has two pieces; otherwise, the curve is composed of one single piece.

For $\theta_C \in [\phi_1, \alpha]$, as depicted in Figure 5b, the lower bound of $\theta_S$ is indicated by point $a$ of straight line segment $abc'$ (i.e., intermediate configuration), where $c'$ is the intersection point between the circular arc centered at $b$ and obstacle line segment $s$. If no intersection occurs between the circular arc and obstacle line segment $s$, then the lower bound of $\theta_S$ is given by point $a$ of straight line segment $abc'$, where $bc'$ intersects with the endpoint of obstacle line segment $s$ farthest from point $b$.

For $\theta_C \in [\alpha, \phi_2]$, the lower bound of $\theta_S$ is indicated by point $a$ of straight line segment $abc'$, where $bc'$ intersects with the endpoint of obstacle line segment $s$ closest to point $b$ (see Figure 5d). Observe that the lower bound of $\theta_S$ is equivalent to $\theta_C$ when $\theta_C = \phi_2$. A sketch of the corresponding infeasible final configuration space is shown in Figure 6.

**Case 2. Obstacle line segment $s$ outside $C$ and inside $C'$.** As depicted in Figure 7, we only need to worry about computing the lower bound of $\theta_S$ for $\theta_C \in [\phi_1, \phi_2]$, given that the entire negative half of the $\theta_S$-range (i.e., $[\theta_C - \cos^{-1} r/R, \theta_C]$) is feasible for $\theta_C \in [0, \phi_1] \cup [\phi_2, 2\pi)$. The analysis is similar to Case 1 and thus omitted. A sketch of the corresponding infeasible final configuration space is shown in Figure 8.

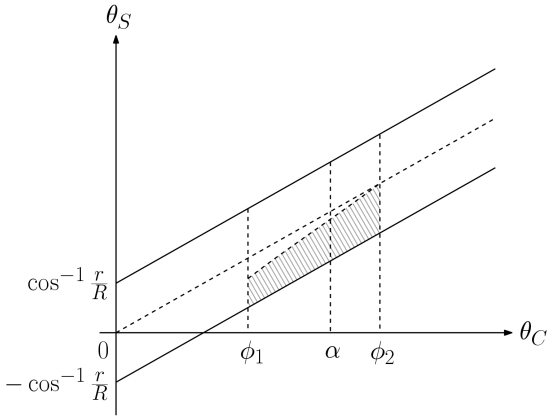


**Figure 6** Infeasible final configuration space due to an obstacle line segment $s$ inside $C$.

## 2.4 Complexity and construction of the feasible trajectory space

The feasible trajectory space of the articulated probe is represented by $\Sigma_{fin} \setminus (\Sigma_{fin,forb} \cup \Sigma_{fin,inf})$. A set of lower- and upper-bound curves – $\sigma_{fin}$, $\sigma_{fin,forb}$, and $\sigma_{fin,inf}$ – was obtained from characterizing the final, forbidden final, and infeasible final configuration spaces, respectively. Each of these curves is a function of $\theta_S$ – that is, $\theta_C(\theta_S)$.

As illustrated in Figure 2, $\sigma_{fin}$ contains two linearly increasing curves, $\theta_C = \theta_S - \cos^{-1} r/R$ and $\theta_C = \theta_S + \cos^{-1} r/R$, which are totally defined over $\theta_S \in [0, 2\pi)$. Each curve in $\sigma_{fin,forb}$ is partially defined, continuous, and monotone in $\theta_S$. Specifically, as shown in Figure 3 & 4, the curves in Case 1 are monotonically decreasing with respect to $\theta_S$, and the curves in Case 2 are of zero slopes (i.e., of some constant $\theta_C$). Furthermore, any two curves in Case 1 can only intersect at most once. Likewise, each curve in $\sigma_{fin,inf}$ is bounded and monotonically increasing with respect to $\theta_S$ (see Figure 6 & 8). Any curve in $\sigma_{fin,inf}$ can only intersect with another at most once.

From the observations above, it can be easily deduced that the number of intersections between any two curves in $\sigma = \sigma_{fin} \cup \sigma_{fin,forb} \cup \sigma_{fin,inf}$ is at most one. In other words, the curves of $\sigma$ are essentially lines, line segments, or pseudo-line segments. For a set $\sigma$ of $O(n)$ $x$-monotone Jordan arcs, bounded or unbounded, with at most $c$ intersections per pair of arcs (for some fixed constant $c$), the maximum combinatorial complexity of the arrangement $A(\sigma)$ is $O(n^2)$ [6].

An incremental construction approach, as detailed in [5], can be used to construct arrangement $A(\sigma)$ in $O(n^2\alpha(n))$ time using $O(n^2)$ space, where $\alpha(n)$ is the inverse Ackermann function. By using topological sweep [1] in computing the intersections for a collection of well-behaved curves (e.g., Jordan curves described above), the time and space complexities can be improved to $O(n \log n + k)$ and $O(n + k)$, respectively.

▶ **Theorem 2.1.** *The feasible trajectory space of the articulated probe can be represented as a simple arrangement of maximum combinatorial complexity $k = O(n^2)$ and can be constructed in $O(n \log n + k)$ time using $O(n + k)$ space.*

**Remark.** The analytical approach above, with a slight change of parameterization and some additional data structure, can be used to solve a special case of the circular sector intersection query problem, and the result is summarized in Theorem 2.2.

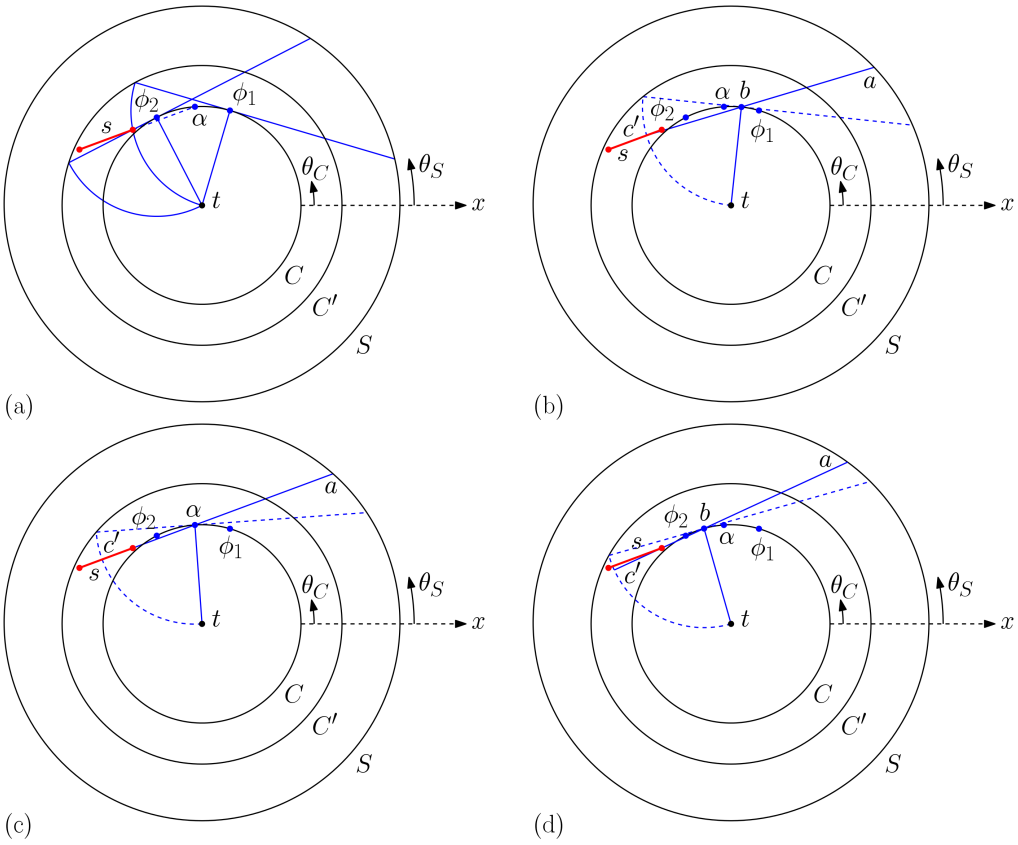


**Figure 7** Infeasible final configurations due to an obstacle line segment $s$ outside $C$ and inside $C'$. Illustration of $\theta_S$-lower bound for (a) $\theta_C \in [\phi_1, \phi_2]$, (b) $\phi_1 < \theta_C < \alpha$, (c) $\theta_C = \alpha$, and (d) $\alpha < \theta_C < \phi_2$.

▶ **Theorem 2.2.** *A set $P$ of $n$ line segments in $\Re^2$ can be preprocessed in $O(n \log n)$ time into a data structure of size $O(n\alpha(n))$ so that, for a query circular sector $\sigma$ with a fixed radius $r$ and a fixed arc endpoint $t$, one can determine if $\sigma$ intersects $P$ in $O(\log n)$ time.*

## References


1. Ivan J Balaban. An optimal algorithm for finding segments intersections. In *Proceedings of the eleventh annual symposium on Computational geometry*, pages 211–219, 1995.
2. Robert Connelly and Erik D Demaine. Geometry and topology of polygonal linkages. *Handbook of Discrete and Computational Geometry*, pages 233–256, 2017.
3. Ovidiu Daescu, Kyle Fox, and Ka Yaw Teo. Computing trajectory with clearance for an articulated probe. In *28th Annual Fall Workshop on Computational Geometry*, 2018.
4. Ovidiu Daescu, Kyle Fox, and Ka Yaw Teo. Trajectory planning for an articulated probe. In *30th Annual Canadian Conference on Computational Geometry*, pages 296–303, 2018.
5. Herbert Edelsbrunner, Leonidas Guibas, János Pach, Richard Pollack, Raimund Seidel, and Micha Sharir. Arrangements of curves in the plane – topology, combinatorics, and algorithms. *Theoretical Computer Science*, 92(2):319–336, 1992.
6. Dan Halperin and Micha Sharir. Arrangements. *Handbook of Discrete and Computational Geometry*, pages 723–762, 2017.

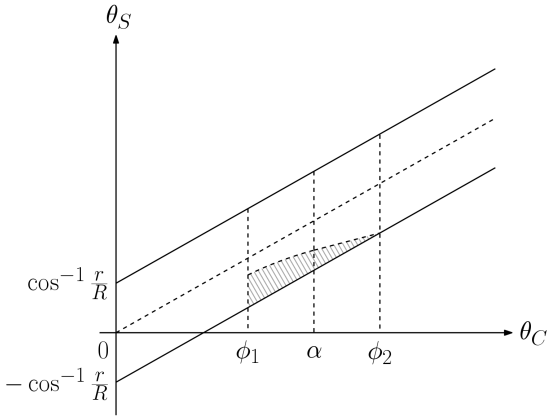


**Figure 8** Infeasible space due to a line segment $s$ outside $C$ and inside $C'$.


7 John Hershberger. Finding the upper envelope of $n$ line segments in $O(n \log n)$ time. *Information Processing Letters*, 33(4):169–174, 1989.

8 John Hopcroft, Deborah Joseph, and Sue Whitesides. Movement problems for 2-dimensional linkages. *SIAM Journal on Computing*, 13(3):610–629, 1984.

9 Steven M LaValle. *Planning algorithms*. Cambridge University Press, 2006.

10 Micha Sharir and Pankaj K Agarwal. *Davenport-Schinzel sequences and their geometric applications*. Cambridge University Press, 1995.